Comparison of Readout-Segmented and Conventional Single-Shot for Echo-Planar Diffusion-Weighted Imaging in the Assessment of Kidney Interstitial Fibrosis

Iris Friedli, MS,[1]* Lindsey Alexandra Crowe, PhD,[1] Thomas de Perrot, MD,[1] Lena Berchtold, MD,[2] Pierre-Yves Martin, MD,[2] Sophie de Seigneux, MD, PhD,[2] and Jean-Paul Vallée, MD, PhD[1]

Purpose: To compare readout-segmented echo-planar imaging (EPI) (RESOLVE) to single-shot EPI (ss-EPI) diffusion-weighted imaging (DWI) for the assessment of renal interstitial fibrosis.
Materials and Methods: A phantom, eight healthy volunteers (under 30 years to avoid age-fibrosis related) and 27 chronic kidney disease (CKD) patients (scheduled for kidney biopsy) were scanned (at 3T) with ss-EPI and 5-shot RESOLVE DWI (resolution: $2 \times 2 \times 5\,mm^3$, 10 b-values). The cortico-medullary difference for each DW parameter from a monoexponential fit (ΔADC) or, segmented biexponential fit (ΔD, ΔD*, ΔF_p) were compared between both sequences. A fibrosis threshold of 40% was defined to separate all 35 subjects into low and high fibrosis groups. The linear relationship between DW parameters and percentage fibrosis (up to 80%) from Masson trichrome was assessed with the Pearson product-moment correlation coefficient. Fisher Z-transform was used for R^2 correlation comparison.
Results: A coefficient of variation between ADCs of 3% was measured between both sequences in the phantom. In healthy volunteers, no significant difference was measured for all DW parameters. Both sequences separated low to high level of fibrosis with a significant decrease of ΔADC (RESOLVE $P = 3.1 \times 10^{-6}$, ss-EPI $P = 0.003$) and ΔD (RESOLVE $P = 8.2 \times 10^{-5}$, ss-EPI $P = 0.02$) in the high level of fibrosis. However, RESOLVE ΔADC had a stronger negative correlation ($P = 0.04$ for R^2 comparison) with fibrosis than ss-EPI ΔADC (RESOLVE $R^2 = 0.65$, $P = 5.9 \times 10^{-9}$, ss-EPI $R^2 = 0.29$, $P = 8.9 \times 10^{-4}$). ΔD (RESOLVE) was correlated (moderately) with fibrosis ($R^2 = 0.29$, $P = 9.2 \times 10^{-4}$); however, ΔD* and ΔF_p did not show, in our population, a significant correlation with interstitial fibrosis ($0.01 < R^2 < 0.08$).
Conclusion: ΔADC derived from both sequences correlated with fibrosis. ΔADC from RESOLVE showed better correlation with fibrosis than ΔADC from ss-EPI and therefore has potential to monitor CKD.
Level of Evidence: 1
Technical Efficacy: Stage 2

J. MAGN. RESON. IMAGING 2017;46:1631–1640.

Chronic kidney disease (CKD) is defined as an alteration of kidney structure and/or function lasting for more than 3 months.[1] The prevalence of CKD is high, with about 1 in 10 adults suffering from some degree of CKD.[2] The level of kidney cortical interstitial fibrosis (from now on referred to as interstitial fibrosis) is recognized as an indicator of impaired renal function and is also predictive of a more serious evolution in most kidney diseases.[3] Renal interstitial fibrosis is characterized by changes in the interstitial space, such as a deposition of extracellular collagen and the destruction of renal tubules and interstitial capillaries.[4] Currently, the gold standard to evaluate these structural alterations is kidney biopsy. However, this procedure is difficult to perform repeatedly and is associated with a risk of hemorrhage as well as sampling bias. There is currently no validated noninvasive method to diagnose and monitor renal interstitial fibrosis.[5]

View this article online at wileyonlinelibrary.com. DOI: 10.1002/jmri.25687

Received Jan 6, 2017, Accepted for publication Feb 13, 2017.

*Address reprint requests to: I.F., Department of Radiology, Geneva University Hospitals, Rue Gabrielle-Perret-Gentil 4,1205 Geneva, Switzerland. E-mail: Iris.Friedli@unige.ch

From the [1]Division of Radiology, Geneva University Hospitals, University of Geneva, Faculty of Medicine, Geneva, Switzerland; and [2]Division of Nephrology, Geneva University Hospitals, University of Geneva, Faculty of Medicine, Geneva, Switzerland

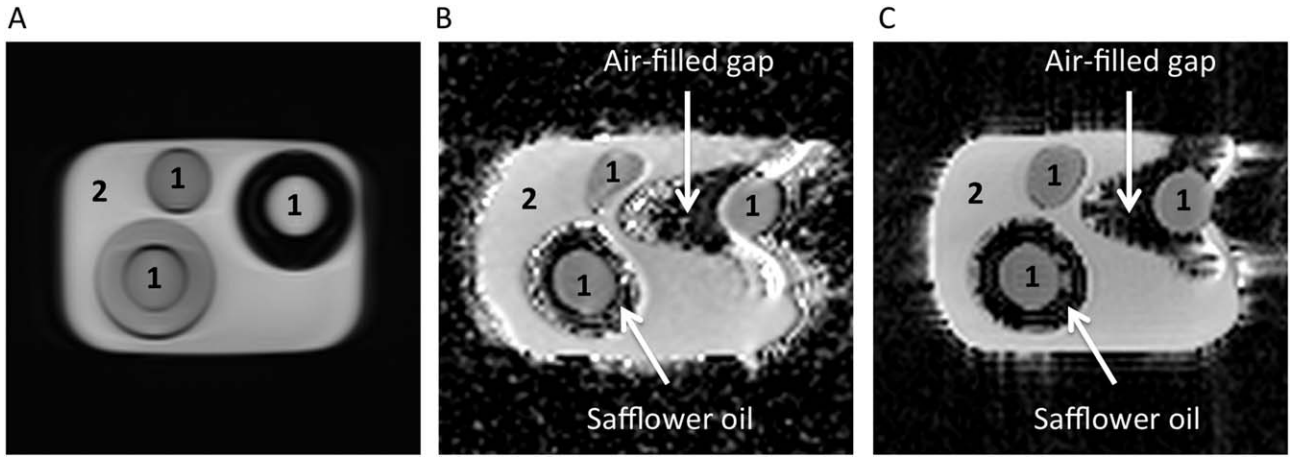

FIGURE 1: Phantom for DWI comparison between ss-EPI and RESOLVE sequences. A: HASTE sequence used as reference for true geometry. B: ADC map calculated with the ss-EPI sequence. C: ADC map from the RESOLVE sequence. Strong distortions are more visible on ss-EPI than RESOLVE, especially in two tubes of compartment 1 encapsulated by or close to the air-filled gap.

Magnetic resonance imaging (MRI) with diffusion-weighted imaging (DWI) is emerging as a tool to assess renal interstitial fibrosis. DWI enables assessment of water molecule mobility via quantification of parameters such as the apparent diffusion coefficient (ADC), the most widely used, from a monoexponential fit, as well as pure diffusion (D), perfusion-induced pseudodiffusion (D*), and perfusion fraction (F_p) coefficients from a biexponential fit. ADC from DWI correlates with interstitial fibrosis in CKD patients and animal models[6–8] and carries potential to change the diagnostic work-up and follow-up of CKD patients. However, ADC measurements are technically challenging and highly variable. Generally, renal DWI is performed using a single-shot *k*-space trajectory, namely, single-shot echo-planar imaging (ss-EPI), which suffers from artifacts due to a long echo train length (ETL).[9] Off-resonance and T_2^* blurring artifacts associated with the long ETL can be reduced by increasing the receiver bandwidth and by the use of parallel imaging techniques such as generalized autocalibrating partially parallel acquisitions (GRAPPA) to reduce the echo spacing. However, this combination, although improving the DW image quality, is not sufficient for renal applications when higher resolution is required as, for example, to differentiate cortex and medulla.[10] The readout segmentation of long variable echo train (RESOLVE) strategy has been proposed to improve the quality of DWI. With this technique, Porter and Heidemann showed a reduction of the signal blurring due to the T_2^* decay during the echo-train in the phase-encoding direction.[11] In this encoding scheme, *k*-space is divided into several shots along the readout direction in order to shorten the echo train length, leading to a longer acquisition time (approximately multiplied by the number of shots) compared to traditional ss-EPI DWI. Recently, improvements in renal interstitial fibrosis assessment was obtained by the use of the RESOLVE sequence associated with the cortico-medullary ADC difference (ΔADC) parameter.[12] ΔADC derived from the RESOLVE sequence was used as a marker to detect a level of more than 40% interstitial fibrosis. In a homogenous population of kidney allograft patients undergoing biopsy, those with more than 40% interstitial fibrosis harbored a negative ΔADC, while a positive ΔADC was measured in patients with less than 40% interstitial fibrosis. Therefore, RESOLVE-derived ΔADC has a strong potential for clinical applications. However, the RESOLVE sequence is significantly longer than ss-EPI, which could be particularly disadvantageous in the abdomen, where respiratory triggering is mandatory. It is not known if the observed good correlation between ΔADC and interstitial fibrosis[12] would still be valid with an MR sequence of shorter acquisition time, ie, ss-EPI. Therefore, the aim of the present study was to compare RESOLVE and ss-EPI DW sequences for the assessment of renal interstitial fibrosis.

Materials and Methods

Phantom

A home-made DWI phantom inspired by Lavdas et al[13] was built to assess ADC quantification of ss-EPI and RESOLVE in a stable and reproducible manner. A plastic container of $14 \times 10 \times 9\,cm^3$ containing three plastic tubes was filled with nickel-doped agarose/sucrose gel. One tube was surrounded by a safflower oil-filled gap, and the second tube by an air-filled gap. The gel in the plastic container and tubes had two distinct ADC values (referred to as "1" and "2" as shown in Fig. 1).

Subjects

This study was performed according to the Declaration of Helsinki and the local Institutional Ethical Committee. Written informed consent for the MRI procedures was obtained from each subject. Eight healthy volunteers (three females and five males, with a mean age of 26 ± 2 years [23–29 years]), without known kidney disease or urinary system disease, and with an upper age limit of 30 years to avoid age-fibrosis related, were recruited.

A cohort of 27 CKD patients (2 native kidney, 25 kidney allografts) planned for a clinically driven kidney biopsy (9 females

and 18 males, with a mean age of 53 ± 10 years [31–83 years]) was scanned with the same protocol as healthy volunteers. All CKD patients underwent, on the same afternoon, a research MRI examination, including a RESOLVE and ss-EPI DW sequences, in addition to the renal biopsy. Those acquiring and analyzing the MRI examinations were blinded for medical history and renal pathology assessment. As a subset analysis, the ADC from RESOLVE and the percentage of fibrosis from the first 25 kidney allograft recipients has already been published.[12] Interstitial fibrosis was quantified histologically by a clinical pathologist (25 years of experience) and graded as a percentage from Masson trichrome staining. The percentage of cortical interstitial fibrosis derived from this examination of the kidney biopsy was considered the reference standard.

MRI

MRI was carried out on a 3T clinical Siemens Magnetom Trio (Tim system) scanner (Siemens, Erlangen, Germany) with a combination of the six elements phased-array abdominal coil and the integrated spine coil. The same protocol and coils were used for both phantom and subjects. For morphological images, 10 pseudo-coronal slices with the same spatial resolution and orientation as for DWI were acquired with both a T_2-weighted Half Fourier acquisition single shot turbo spin echo (HASTE) and modified Look-Locker inversion recovery (MOLLI) T_1 mapping sequence.[14] For the functional DWI assessment, the protocol included a navigator-triggered echo planar imaging (EPI) based single-shot readout MR scan (ss-EPI) using PACE (prospective acquisition correction technique) and a RESOLVE[10,11] diffusion-weighted SE-EPI (spin echo based EPI) acquisition synchronized to the patient respiration, using a respiratory belt wrapped around the abdomen. For both ss-EPI and RESOLVE, the sequence parameters were TE/TR = 68/2200 msec, spatial resolution = 2 × 2 × 5 mm^3, parallel imaging (generalized autocalibrating partially parallel acquisitions, GRAPPA) factor = 3, a bipolar diffusion scheme with the diffusion-encoding gradients applied in three orthogonal directions and 10 b-values (0, 10, 20, 40, 60, 150, 300, 500, 700, and 900 s/mm^2). Shim settings and spatial resolution were strictly identical for all MR sequences. The five shot RESOLVE acquisition reduced echo spacing to 0.32 msec from 0.69 msec (ss-EPI) and increased acquisition time to 9′47″ ± 4′ as compared to the ss-EPI at 2′20″ ± 1′17″ depending on respiration.

Image Analysis and Data Fitting

MR analysis was performed blinded to histologic results. Freehand regions of interests (ROIs) were manually placed for quantification of both the cortex and medulla as previously described.[12] In brief, two to three cortical ROIs followed the outer contour of the kidney and three medullary ROIs were traced on the T_1 maps and copied on b_0 images, avoiding artifacts, lesions, and major vessels. Signal intensity values inside ROIs were exported as .csv files with the OsiriX "export ROI" tool plugin and analyzed with MatLab (R2012b, MathWorks, Natick, MA) for diffusion data fitting using a Levenberg-Marquardt algorithm. The apparent diffusion coefficient (ADC) was calculated using a nonlinear least square method for the monoexponential fitting according to the following formula:

$$ADC = \frac{1}{b}\log\left(\frac{S_0}{S_i}\right) \quad (1)$$

where S_i is the signal intensity measured on the i^{th} b-value image and S_0 is the signal amplitude in the absence of diffusion weighting (b = 0 s/mm^2). To separate the molecular diffusion from the microcirculation of blood in the capillary network (perfusion), the biexponential model[15] was performed using the segmented fitting method[16] with the following formula:

$$\frac{S_i(b)}{S_0} = (1-F_p)e^{-b_i \cdot D} + F_p e^{-b_i \cdot (D^* + D)} \quad (2)$$

where D is the diffusion coefficient representing "pure" molecular diffusion (slow component), D* is the perfusion-induced pseudo-diffusion coefficient (fast component), and F_p is the perfusion fraction, ie, the fraction of the signal intensity S_0 attributed to capillary blood flowing in each voxel (%). Considering that $D^* \gg D$, the influence of D* on signal decay was neglected for b > 200 s/mm^2. Therefore, D was first determined from monoexponential data fitting of the four highest b-values (b = 300, 500, 700, 900 s/mm^2) according to the following equation:

$$S_i(b) = S_{int} \cdot e^{-b_i \cdot D} \quad (3)$$

where S_{int} is the b_0 intercept of the monoexponential fit of high b-value data. Then, F_p was calculated as:

$$F_p = \frac{S_0 - S_{int}}{S_0} \quad (4)$$

These values of D and F_p were then fixed, and D* was calculated using a partially constrained non-linear regression of all data sets according to Eq. [2].

In all subjects (healthy volunteers and CKD patients), the cortico-medullary difference of each DW parameter (ΔADC, ΔD, ΔD*, and ΔF_p) was defined in order to minimize interindividual variations. DW parameters were expressed as mean value in the ROIs ± standard deviation.

Data Analysis

Phantom results allowed us to quantify the ADC variability between DW sequences in stable and reproducible conditions. ROIs were manually drawn within the two different compartments using OsiriX software (http://www.osirix-viewer.com/). ADC comparison between (i) ss-EPI and (j) RESOLVE sequences was done using the coefficient of variation CV [%] expressed as:

$$CV(i,j) = \frac{\sigma_{ADC(i,j)}}{\mu_{ADC(i,j)}} \times 100 \quad (5)$$

Comparison between ss-EPI and RESOLVE sequences was done in healthy volunteers, with a paired *t*-test between mean ΔDW parameters. An experienced uroradiologist (20 years) was consulted to ensure the quality of images for diagnostic purposes.

A fibrosis threshold of 40% was selected, as reported previously,[12] to separate all subjects (healthy volunteers and CKD

TABLE 1. ADC Values Measured in the Phantom for DWI with ss-EPI and RESOLVE Sequences

	RESOLVE Mean ADC Values (σ) [$10^{-6}mm^2/s$]		ss-EPI Mean ADC Values (σ) [$10^{-6}mm^2/s$]	
Compartment "1"	1287	(45)	1359	(97)
Compartment "2"	1890	(34)	1903	(25)

patients) into two groups according to the level of fibrosis: one group (low to moderate fibrosis group) with a level of interstitial fibrosis lower than 40% ($n = 28$) and the second group (high fibrosis group) with more than 40% ($n = 7$). Welch's two-sample *t*-test was computed between groups for DWI parameters of ss-EPI and RESOLVE sequences. The limit of 40% of interstitial fibrosis was also used to stratify the area under the curves (AUC) of the receiver operating characteristics (ROC). ROC curves, plotting the true positive versus the false positive prediction rates, were used to assess the discrimination power of ΔADC of ss-EPI and RESOLVE sequences. ROC curves were considered "paired." Comparison between them was based on AUCs and done with the DeLong method,[17] available in the package pROC[18] of R software (v. 0.98.1091). The linear relationship between DWI parameters of both MR sequences and interstitial fibrosis was tested using the Pearson product-moment correlation coefficient. Linear correlations with $P < 0.05$ were considered as moderate at $R^2 > 0.20$ and strong at $R^2 > 0.45$. The significance of the difference between correlation coefficients was performed using the Fisher Z-transform. A *P*-value of less than 0.05 was considered to indicate a statistically significant difference.

Results

Phantom

Compared to images from the RESOLVE sequence, the ADC map from ss-EPI showed more susceptibility artifacts due to the air-filled compartment, as shown in Fig. 1. However, no differences were found between ss-EPI and RESOLVE sequences for quantification of ADC when measured in the center of the phantom free of artifacts. Mean ADC values of each compartment are shown in Table 1. A coefficient of variation (CV) less than 3% was measured between the two DW sequences.

Healthy Volunteers

A cortico-medullary contrast with a positive ΔADC, as shown in Fig. 2A, was measured with both DW sequences. In healthy volunteers, ss-EPI and RESOLVE sequences had no significant difference between DW parameters, as shown in Table 2.

Interstitial Fibrosis Assessment

The level of interstitial fibrosis measured in CKD patients from Masson trichrome ranged from 0–80% with a mean interstitial fibrosis of $31 \pm 20\%$. An example of b_0 image and ADC, D, and D* maps obtained from ss-EPI and RESOLVE sequences in a CKD patient with 30% of interstitial fibrosis is shown in Fig. 2B. During assessment for diagnostic quality it was observed that, compared to healthy volunteers, a loss of cortico-medullary differentiation was visible on both DW sequences in all patients with a high level of interstitial fibrosis.

For both DW sequences, ΔADC was significantly lower in the high fibrosis group compared to the low fibrosis group ($P = 0.003$ for ss-EPI and $P = 3.1 \times 10^{-6}$ for RESOLVE). The RESOLVE sequence with ΔADC led to a specificity and sensitivity of 100% and 86%, and the ss-EPI led to a specificity of 82% and sensitivity of 86% but, no significant difference of AUCs was measured between ss-EPI and RESOLVE using the fibrosis threshold of 40%, as shown in Fig. 3 ($P = 0.16$ between AUCs of ss-EPI and RESOLVE with the Delong method).

ΔADC from both DW sequences was linearly correlated with the percentage of fibrosis, as shown in Fig. 4A. ΔADC from RESOLVE had a significantly better correlation with interstitial fibrosis than ΔADC obtained with ss-EPI ($P = 0.04$, according to R^2 correlation comparison using the Fisher Z-transform).

Regarding the biexponential fitting parameters, a significant decrease of mean ΔD was measured in the high fibrosis group compared to the low fibrosis group for both sequences ($P = 0.02$ for ss-EPI and $P = 8.2 \times 10^{-5}$ for RESOLVE). However, for the remaining parameters (D* and F_p), no statistical difference was found between low and high fibrosis groups for either sequence. Regarding the correlation with interstitial fibrosis, only ΔD measured with the RESOLVE sequence was linearly related with renal interstitial fibrosis, as shown in Fig. 4B ($R^2 = 0.29$, $P = 9.2 \times 10^{-4}$). No statistical correlation was found with any of the DW parameters derived from the ss-EPI sequence and interstitial fibrosis (ΔD: $R^2 = 0.12$, ΔD*: $R^2 = 0.08$, ΔF_p: $R^2 = 0.01$).

Discussion

The main result of this study is that the RESOLVE sequence derived ΔADC (ADC cortico-medullary difference) was superior to ss-EPI-derived ΔADC, as shown by a stronger linear correlation with the percentage of fibrosis from biopsy.

In the present study, we extended previous comparison of RESOLVE and ss-EPI sequences that were based only on image quality analysis[10] by including a comparison of DW parameters in a phantom and CKD patients. In the center of the gel phantom in a region free of susceptibility artifacts, no ADC difference was measured between ss-EPI and RESOLVE sequences, attesting the absence of systematic bias between both sequences.

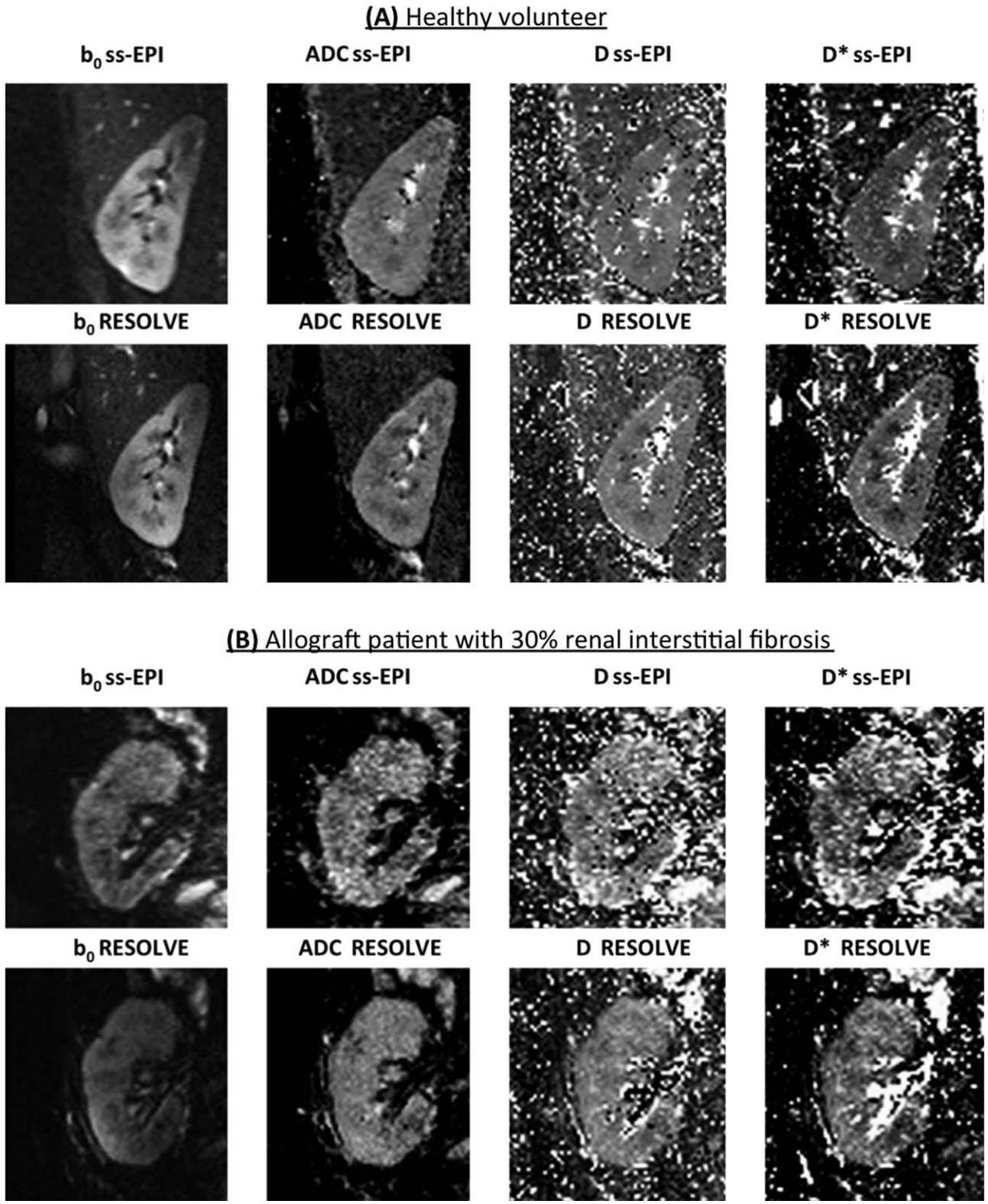

FIGURE 2: Example of coronal MR images (b_0, ADC, D, and D* maps) of the right kidney of (A) a 26-year-old female healthy volunteer and of (B) an 83-year-old allograft patient with 30% interstitial fibrosis. First row are images obtained from the ss-EPI sequence and the second row are those obtained with the RESOLVE sequence. Cortico medullary differences were visible in healthy volunteer but disappeared in CKD with 30% of fibrosis DWI maps.

However, the in vivo comparison demonstrated a clear advantage of the RESOLVE sequence over the ss-EPI sequence.

Several studies had previously found an improvement of the global DW image quality with the RESOLVE strategy due mainly to reduced T_2^* blurring and susceptibility

TABLE 2. Comparison of DW Parameters for ss-EPI and RESOLVE in 8 Healthy Volunteers

	RESOLVE mean values (σ)		ss-EPI mean values (σ)		*P*-values
ADC cortex [10^{-6}mm^2/s]	2250	(155)	2229	(173)	0.83
ADC medulla [10^{-6}mm^2/s]	1983	(161)	2046	(166)	0.47
ΔADC [10^{-6}mm^2/s]	267	(86)	183	(100)	0.28
D cortex [10^{-6}mm^2/s]	1788	(117)	1955	(162)	0.12
D medulla [10^{-6}mm^2/s]	1634	(88)	1849	(189)	0.08
ΔD [10^{-6}mm^2/s]	154	(109)	106	(58)	0.4
D* cortex [10^{-6}mm^2/s]	35704	(12563)	37621	(18159)	0.9
D* medulla [10^{-6}mm^2/s]	31508	(12787)	41613	(26793)	0.46
ΔD* [10^{-6}mm^2/s]	4196	(24561)	-3992	(21680)	0.68
Fp cortex [%]	23	(8)	16	(8)	0.19
Fp medulla [%]	18	(8)	16	(8)	0.66
Δ Fp [%]	5	(8)	0.25	(9)	0.46

No significant difference in all DW parameters was seen between ss-EPI and RESOLVE sequences. $P > 0.05$ for all parameters/markers.

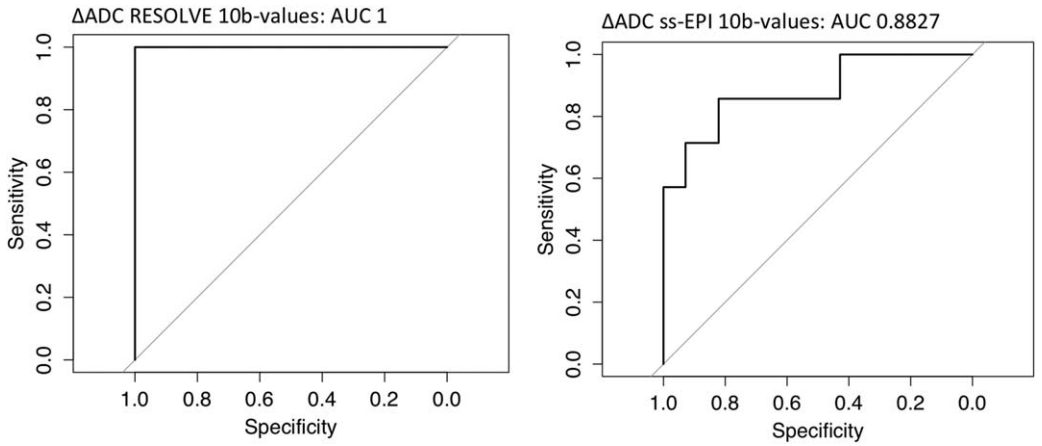

FIGURE 3: AUC of the ROC using 40% of interstitial fibrosis as a limit for renal fibrosis detection by ΔADC. All patients with more than 40% of interstitial fibrosis had a negative ΔADC, whereas all patients with less than 40% had a positive ΔADC, resulting in an AUC from the RESOLVE sequence obtained with 10 b-values equal to 1. A weaker ability to separate a high level and low level of fibrosis was measured with the ss-EPI sequence with a reduced AUC, attesting the presence of true positive and/or false positive. However, no significant difference of AUCs was measured between ss-EPI and RESOLVE using the fibrosis threshold of 40%.

effects, mainly resulting in an enhancement of tumor lesion detection in various organs, such as head and neck region,[19,20] breast,[21–23] pelvis,[24] thyroid,[25] and rectum.[26] All these studies showed that the greater tumor lesion to normal tissue contrast from RESOLVE resulted in a better ADC differentiation of healthy tissues and tumors. Except in one study of the parotid glands,[20] which showed no significant difference in tumoral ADC values between RESOLVE and ss-EPI, a significantly lower ADC value was always measured with the readout-segmented strategy within malignant lesions in all these other studies. In our study, a larger negative ΔADC was measured with RESOLVE by comparison to ss-EPI in patients with more than 40% of interstitial fibrosis. The explanation of this ADC difference between RESOLVE and ss-EPI measured in pathologies, but not seen in healthy tissues, is still unclear and under debate. The better delineation of lesions by the RESOLVE sequence[21–23,27–30] could decrease the averaging with adjacent high ADC values of normal tissues and, thus, preserve the lower ADC values in the tumor as observed in breast cancer.[22] However, Zhao et al[31] contested that adjacent

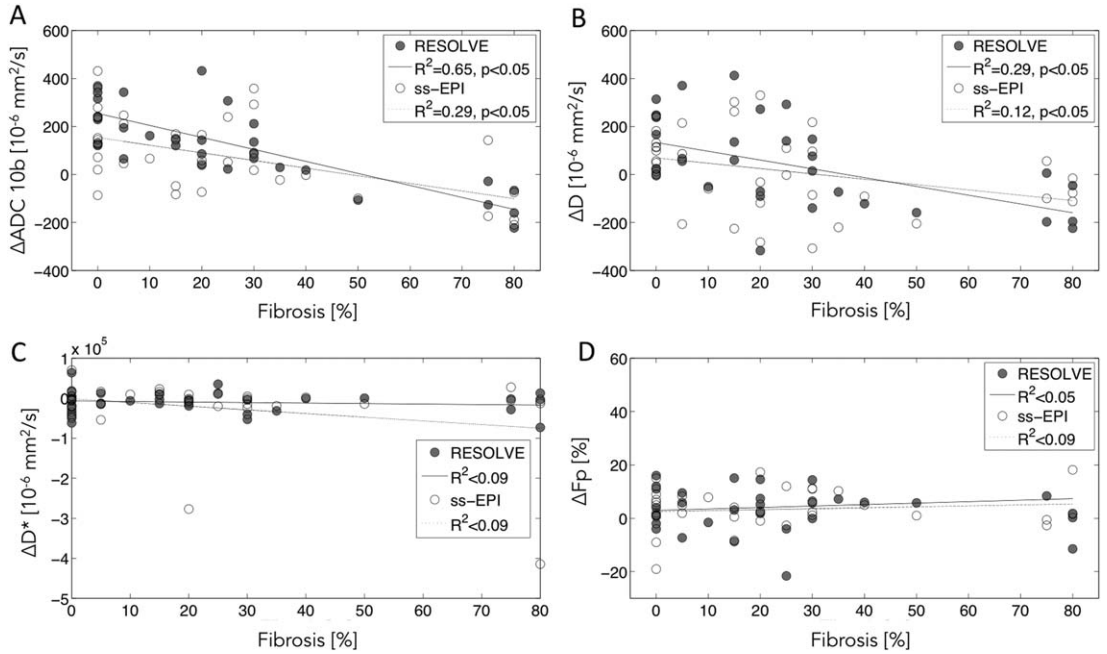

FIGURE 4: Correlations between ΔADC (A), ΔD (B), ΔD* (C), ΔF_p (D) and renal interstitial fibrosis from ss-EPI and RESOLVE sequences. Data were acquired from 35 subjects (27 CKD patients and eight healthy volunteers). ΔADC from RESOLVE was better correlated to renal interstitial fibrosis than ΔADC from ss-EPI ($P = 0.04$ by R^2 correlation comparison using the Fisher Z-transform). Regarding biexponential fitting parameters, correlations between ΔD and renal interstitial fibrosis were observed for the RESOLVE sequence only. ΔADC from ss-EPI and ΔD from RESOLVE gave equivalent correlation with the percentage of fibrosis. All other correlations were not significant, suggesting that the intravoxel incoherent motion parameters of perfusion (ΔD*) and fraction of perfusion (ΔF_p) were not linked to renal interstitial fibrosis in our population.

high ADC values of normal tissues could impact the ADC values measured in the lesion. They compared in terms of ADC values, RESOLVE, and ss-EPI in the brainstem and sinonasal lesions. The sinonasal lesions, which were not surrounded by high ADC values of normal tissues, had significantly lower ADC values on RESOLVE compared to ss-EPI. By contrast, the brainstem measurements, less affected by the susceptibility artifacts and ghosts than sinonasal lesions, exhibited no significant differences between the two DW sequences. They concluded that the difference in ADC values could be more attributed to susceptibility artifacts and ghosts, present in the sinonasal lesions DW images, than by adjacent high ADC values of normal tissues. In our case, both effects (ie, a reduction of susceptibility effects preserving the cortex from artifacts and an improved anatomical delineation) could explain the better performance of the RESOLVE sequence.

The biexponential-fitting values measured in the current study had comparable values with those reported in previous studies on kidney allograft patients,[32,33] but did not allow us to discriminate the level of interstitial fibrosis. The biexponential-fitting parameters with either the ss-EPI or RESOLVE sequence were not significantly correlated with the percentage of fibrosis from biopsy. We therefore concluded that the biexponential model is inadequate to robustly assess the percentage of kidney fibrosis in our population. This result was consistent with another study, which found an absence of correlation in diffuse liver fibrosis.[34] In addition, biexponential parameters in the kidney have been shown not to correlate significantly with enhanced glomerular filtration rate (eGFR),[35,36] which is in turn correlated with renal interstitial fibrosis.[12] The major difficulties of using a biexponential fitting are the large variability in the resulting parameters and the lack of robustness against noise.[37] Also, despite the use of physiological triggering schemes to limit respiratory artifacts, physiological motion artifacts that lead to inhomogeneous signal dropout can impact kidney images. We might expect that biexponential fitting would be more sensitive to decreases of signal intensity, as more points are needed to build the fit.

An increase of D* has been measured with the increase of eGFR.[33] However, the correlation was relatively weak, probably due to the large variability of D* due to the fitting.[38–40] An interpatient coefficient of variation (CV) of 25% was found for the F_p parameter in a study on the variability of biexponential parameters in renal allograft patient after transplantation (5–19 days).[41] Despite the use of the cortico-medullary difference and the RESOLVE sequence, which reduced intersubject variability compared to the cortical or medullary ADC, we found that biexponential parameters with ΔD, ΔD^*, and ΔF_p did not accurately assess renal fibrosis. The relevance of the biexponential model in general is still subject to debate.

There are some inherent limitations of our study. The size of our population was restricted, especially in terms of patients with a high level of fibrosis (>40%), as few patients with acute kidney disease or CKD and a high level of fibrosis had routine biopsy. Fibrosis in healthy volunteers was not measured, but these subjects were considered to have no fibrosis. This could introduce an additional error; however, such an assumption is valid in a relatively young population, all under 30 years of age, thus avoiding age-related fibrosis. The lack of perfusion in the diffusion phantom limits its use to ADC calculation in stable and reproducible condition and does not allow biexponential fitting parameters assessment. An implementation of Lemke's correction[39] by acquiring T_1 and T_2 maps would be appropriate to take into account T_2 effects and correct the F_p parameter for the biexponential. However, in case of chronic disease, we would not expect a significant difference in T_2 values between subjects, and therefore the uncorrected F_p, while not the true value, could be compared between the DW sequences.

Finally, this study supports the advantages of ΔADC from the RESOLVE sequence to assess renal interstitial fibrosis, despite the longer acquisition time compared to the conventional ss-EPI. An alternative approach would be to acquire the ss-EPI sequence with more averages on b-values such that the scan time would have been equivalent to RESOLVE. This strategy could be used to increase the signal-to-noise ratio and therefore improve ss-EPI analysis. However, this would not correct for off-resonance effects maintaining this disadvantage over RESOLVE. The initial goal of this study was to verify if there is a benefit of using the RESOLVE strategy compared to the inherently shorter acquisition time ss-EPI. It would be worthwhile in future work to verify if reducing the number of b-values could shorten the acquisition time without impacting DWI parameters. Such an analysis is beyond the scope of the current study aiming to compare ss-EPI and RESOLVE with DW parameters obtained with monoexponential and biexponential fitting for interstitial fibrosis assessment.

In conclusion, ΔADC derived from both RESOLVE and ss-EPI is sensitive to fibrosis. ΔADC from RESOLVE has a significantly better correlation with interstitial fibrosis than ΔADC from ss-EPI. Biexponential-fitting parameters showed no advantage for renal interstitial fibrosis assessment for either sequence. Despite a longer acquisition time compared to ss-EPI, the use of the RESOLVE sequence with ΔADC calculation to assess renal interstitial fibrosis is therefore recommended.

Acknowledgments

Contract grant sponsor: Swiss National Foundation; contract grant number: FNS 32003B_159714/1 (ME10250); Contract grant sponsor: Clinical Research Center of the Medicine Faculty of Geneva University and Geneva University Hospital; Contract grant sponsor: Centre For Biomedical Imaging (CIBM).

References

1. Levey AS, Coresh J. Chronic kidney disease. Lancet 2012;379: 165–180.
2. Ponte B, Pruijm M, Marques-Vidal P, et al. Determinants and burden of chronic kidney disease in the population-based CoLaus study: a cross-sectional analysis. Nephrol Dial Transpl 2013;28: 2329–2339.
3. Toki D, Inui M, Ishida H, et al. Interstitial fibrosis is the critical determinant of impaired renal function in transplant glomerulopathy. Nephrology 2016;21(Suppl 1):20–25.
4. Boor P, Ostendorf T, Floege J. Renal fibrosis: novel insights into mechanisms and therapeutic targets. Nat Rev Nephrol 2010;6: 643–656.
5. Boor P, Floege J. Chronic kidney disease growth factors in renal fibrosis. Clin Exp Pharmacol Physiol 2011;38:441–450.
6. Inoue T, Kozawa E, Okada H, et al. Noninvasive evaluation of kidney hypoxia and fibrosis using magnetic resonance imaging. J Am Soc Nephrol 2011;22:1429–1434.
7. Zhao J, Wang ZJ, Liu M, et al. Assessment of renal fibrosis in chronic kidney disease using diffusion-weighted MRI. Clin Radiol 2014;69: 1117–1122.
8. Hueper K, Khalifa AA, Brasen JH, et al. Diffusion-Weighted imaging and diffusion tensor imaging detect delayed graft function and correlate with allograft fibrosis in patients early after kidney transplantation. J Magn Reson Imaging 2016;44:112–121.
9. Le Bihan D, Poupon C, Amadon A, Lethimonnier F. Artifacts and pitfalls in diffusion MRI. J Magn Reson Imaging 2006;24:478–488.
10. Friedli I, Crowe LA, Viallon M, et al. Improvement of renal diffusion-weighted magnetic resonance imaging with readout-segmented echo-planar imaging at 3T. Magn Reson Imaging 2015; 33:701–708.
11. Porter DA, Heidemann RM. High resolution diffusion-weighted imaging using readout-segmented echo-planar imaging, parallel imaging and a two-dimensional navigator-based reacquisition. Magn Reson Med 2009;62:468–475.
12. Friedli I, Crowe LA, Berchtold L, et al. New magnetic resonance imaging index for renal fibrosis assessment: a comparison between diffusion-weighted imaging and T1 mapping with histological validation. Sci Rep 2016;6:30088.
13. Lavdas I, Behan KC, Papadaki A, McRobbie DW, Aboagye EO. A phantom for diffusion-weighted MRI (DW-MRI). J Magn Reson Imaging 2013;38:173–179.
14. Messroghli DR, Radjenovic A, Kozerke S, Higgins DM, Sivananthan MU, Ridgway JP. Modified Look-Locker inversion recovery (MOLLI) for high-resolution T1 mapping of the heart. Magn Reson Med 2004;52: 141–146.
15. Le Bihan D, Breton E, Lallemand D, Aubin ML, Vignaud J, Laval-Jeantet M. Separation of diffusion and perfusion in intravoxel incoherent motion MR imaging. Radiology 1988;168:497–505.
16. Schneider MJ, Dietrich O, Ingrisch M, et al. Intravoxel incoherent motion magnetic resonance imaging in partially nephrectomized kidneys. Invest Radiol 2016;51:323–330.
17. DeLong ER, DeLong DM, Clarke-Pearson DL. Comparing the areas under two or more correlated receiver operating characteristic curves: a nonparametric approach. Biometrics 1988;44:837–845.
18. Robin X, Turck N, Hainard A, et al. pROC: an open-source package for R and S+to analyze and compare ROC curves. BMC Bioinform 2011;12:77.
19. Yeom KW, Holdsworth SJ, Van AT, et al. Comparison of readout-segmented echo-planar imaging (EPI) and single-shot EPI in clinical application of diffusion-weighted imaging of the pediatric brain. AJR Am J Roentgenol 2013;200:W437–443.
20. Koyasu S, Iima M, Umeoka S, et al. The clinical utility of reduced-distortion readout-segmented echo-planar imaging in the head and neck region: initial experience. Eur Radiol 2014;24: 3088–3096.
21. Bogner W, Pinker-Domenig K, Bickel H, et al. Readout-segmented echo-planar imaging improves the diagnostic performance of diffusion-weighted MR breast examinations at 3.0 T. Radiology 2012; 263:64–76.
22. Wisner DJ, Rogers N, Deshpande VS, et al. High-resolution diffusion-weighted imaging for the separation of benign from malignant BI-RADS 4/5 lesions found on breast MRI at 3T. J Magn Reson Imaging 2014;40:674–681.
23. Kim YJ, Kim SH, Kang BJ, et al. Readout-segmented echo-planar imaging in diffusion-weighted mr imaging in breast cancer: comparison with single-shot echo-planar imaging in image quality. Kor J Radiol 2014;15:403–410.
24. Thian YL, Xie W, Porter DA, Weileng Ang B. Readout-segmented echo-planar imaging for diffusion-weighted imaging in the pelvis at 3T—A feasibility study. Acad Radiol 2014;21:531–537.
25. Schob S, Voigt P, Bure L, et al. Diffusion-weighted imaging using a readout-segmented, multishot EPI sequence at 3 T distinguishes between morphologically differentiated and undifferentiated subtypes of thyroid carcinoma—A preliminary study. Transl Oncol 2016;9: 403–410.
26. Xia CC, Liu X, Peng WL, et al. Readout-segmented echo-planar imaging improves the image quality of diffusion-weighted MR imaging in rectal cancer: Comparison with single-shot echo-planar diffusion-weighted sequences. Eur J Radiol 2016;85:1818–1823.
27. Holdsworth SJ, Yeom K, Skare S, Gentles AJ, Barnes PD, Bammer R. Clinical application of readout-segmented-echo-planar imaging for diffusion-weighted imaging in pediatric brain. AJNR Am J Neuroradiol 2011;32:1274–1279.
28. Naganawa S, Yamazaki M, Kawai H, Sone M, Nakashima T, Isoda H. Anatomical details of the brainstem and cranial nerves visualized by high resolution readout-segmented multi-shot echo-planar diffusion-weighted images using unidirectional MPG at 3T. Magn Reson Med Sci 2011;10:269–275.
29. Iima M, Yamamoto A, Brion V, et al. Reduced-distortion diffusion MRI of the craniovertebral junction. AJNR Am J Neuroradiol 2012;33: 1321–1325.
30. Morelli J, Porter D, Ai F, et al. Clinical evaluation of single-shot and readout-segmented diffusion-weighted imaging in stroke patients at 3 T. Acta Radiol 2013;54:299–306.
31. Zhao M, Liu Z, Sha Y, et al. Readout-segmented echo-planar imaging in the evaluation of sinonasal lesions: A comprehensive comparison of image quality in single-shot echo-planar imaging. Magn Reson Imaging 2016;34:166–172.
32. Heusch P, Wittsack HJ, Heusner T, et al. Correlation of biexponential diffusion parameters with arterial spin-labeling perfusion MRI: results in transplanted kidneys. Invest Radiol 2013;48:140–144.
33. Ren T, Wen CL, Chen LH, et al. Evaluation of renal allografts function early after transplantation using intravoxel incoherent motion and arterial spin labeling MRI. Magn Reson Imaging 2016;34:908–914.
34. Franca M, Marti-Bonmati L, Alberich-Bayarri A, et al. Evaluation of fibrosis and inflammation in diffuse liver diseases using intravoxel incoherent motion diffusion-weighted MR imaging. Abdom Radiol 2016 [Epub ahead of print].
35. Bane O, Wagner M, Zhang JL, et al. Assessment of renal function using intravoxel incoherent motion diffusion-weighted imaging and dynamic contrast-enhanced MRI. J Magn Reson Imaging 2016;44: 317–326.
36. Ding J, Chen J, Jiang Z, Zhou H, Di J, Xing W. Assessment of renal dysfunction with diffusion-weighted imaging: comparing intra-voxel incoherent motion (IVIM) with a mono-exponential model. Acta Radiol 2016;57:507–512.
37. Wittsack HJ, Lanzman RS, Mathys C, Janssen H, Modder U, Blondin D. Statistical evaluation of diffusion-weighted imaging of the human kidney. Magn Reson Med 2010;64:616–622.

38. King MD, Vanbruggen N, Busza AL, Houseman J, Williams SR, Gadian DG. Perfusion and diffusion MR imaging. Magn Reson Med 1992;24:288–301.

39. Lemke A, Laun FB, Simon D, Stieltjes B, Schad LR. An in vivo verification of the intravoxel incoherent motion effect in diffusion-weighted imaging of the abdomen. Magn Reson Med 2010; 64:1580–1585.

40. Barbieri S, Donati OF, Froehlich JM, Thoeny HC. Impact of the calculation algorithm on biexponential fitting of diffusion-weighted MRI in upper abdominal organs. Magn Reson Med 2016;75: 2175–2184.

41. Eisenberger U, Thoeny HC, Binser T, et al. Evaluation of renal allograft function early after transplantation with diffusion-weighted MR imaging. Eur Radiol 2010;20:1374–1383.